NANO LETTERS

Letter

pubs.acs.org/NanoLett

# Confined Acoustic Phonons in Colloidal Nanorod Heterostructures Investigated by Nonresonant Raman Spectroscopy and Finite Elements Simulations

Mario Miscuglio,[†,§] Miao-Ling Lin,[‡] Francesco Di Stasio,[†] Ping-Heng Tan,[*,‡] and Roman Krahne[*,†]

[†]Nanochemistry Department, Istituto Italiano di Tecnologia, Via Morego 30, 16163 Genova, Italy

[‡]State Key Laboratory of Superlattices and Microstructures, Institute of Semiconductors, Chinese Academy of Sciences, Beijing 100083, China

[§]Dipartimento di Chimica e Chimica Industriale, Università di Genova, Via Dodecaneso 31, 16146 Genova, Italy

*S* *Supporting Information*

**ABSTRACT:** Lattice vibrational modes in cadmium chalcogenide nanocrystals (NCs) have a strong impact on the carrier dynamics of excitons in such confined systems and on the optical properties of these nanomaterials. A prominent material for light emitting applications are CdSe/CdS core−shell dot-in-rods. Here we present a detailed investigation of the acoustic phonon modes in such dot-in-rods by nonresonant Raman spectroscopy with laser excitation energy lower than their bandgap. With high signal-to-noise ratio in the frequency range from 5−50 $cm^{-1}$, we reveal distinct Raman bands that can be related to confined extensional and radial-breathing modes (RBM). Comparison of the experimental results with finite elements simulation and analytical analysis gives detailed insight into the localized nature of the acoustic vibration modes and their resonant frequencies. In particular, the RBM of dot-in-rods cannot be understood by an oscillation of a CdSe sphere embedded in a CdS rod matrix. Instead, the dot-in-rod architecture leads to a reduction of the sound velocity in the core region of the rod, which results in a redshift of the rod RBM frequency and localization of the phonon induced strain in vicinity of the core where optical transitions occur. Such localized effects potentially can be exploited as a tool to tune exciton−phonon coupling in nanocrystal heterostructures.

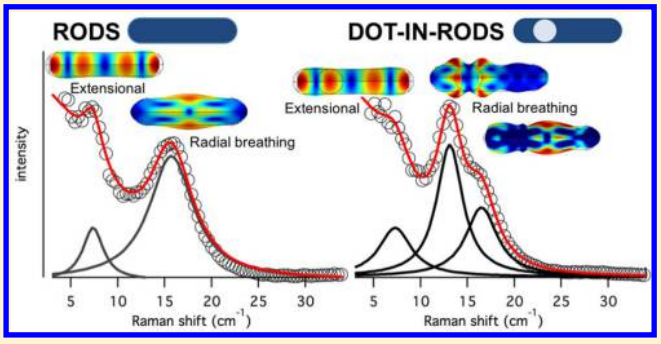


**KEYWORDS:** *Confined acoustic phonons, colloidal nanorod heterostructures, nonresonant Raman spectroscopy, finite elements simulations*

Colloidal semiconductor nanocrystals (NCs) and in particular nanorods have created tremendous interest to date due to their unique optical properties, such as efficient and tunable light emission via size control,[1−3] exciton storage,[4] electroluminescence,[5] and optical gain,[6,7] just to name a few. This has translated to applications as fluorescent markers in biology,[1] emitting materials in electro-optic devices such as LEDs and lasers,[8−14] and key components in next generation displays.[15] One important milestone was the synthesis of core−shell quantum dots and nanorods that contain at least two semiconductors arranged in an onion-like geometry.[16−19] Among these, dot-in-rod core−shell heterostructures fabricated by the seeded growth approach[18,19] have extremely narrow size distributions that result in well-defined optical properties, which can be fine-tuned by control over core size and rod length.[20−24]

Lattice vibrational modes in NCs have a strong impact on the carrier dynamics of excitons in such confined systems and, consequently, on their optical properties.[25−28] Optical and acoustic vibrational modes can be detected by discrete phonon replicas in the emission spectrum of NC ensembles[29−31] and single NCs.[32−36] Acoustic phonon modes are of special interest because they can assist in transitions that are otherwise forbidden, in particular from the bright to dark exciton state.[31,37,38] The acoustic modes are expected from linear elasticity theory to depend strongly on the size and shape, as well as on the strain distribution.[39−44] However, the simplified approach based on Lamb's theory considering solely the radius of the nanostructure that is typically applied[33,36,43,44] should have its limits concerning anisotropic- and core−shell hetero-NCs. Therefore, a detailed experimental and theoretical investigation of ultralow frequency (ULF) Raman modes in core−shell hetero-NCs is essential to understand the fundamental properties of acoustic NC vibrations.

In this letter, acoustic vibrations of CdS nanorods and CdSe/CdS dot-in-rods that consist of a CdSe core and a rod-shaped CdS shell are studied by nonresonant Raman spectroscopy.

**Received:** September 2, 2016
**Revised:** November 15, 2016
**Published:** November 23, 2016





DOI: 10.1021/acs.nanolett.6b03706
*Nano Lett.* 2016, 16, 7664−7670

The phonon modes in the ULF region can be clearly assigned by their polarization behavior and Lamb's theory to extensional and breathing modes of the NCs. In dot-in-rods the dominant RBM is red-shifted with respect to bare nanorods, which can be analyzed quantitatively in terms of local reduction of sound velocity. Finite element simulations using Comsol software reveal the intricate distribution of strain induced by the acoustic vibrations and, particularly, the localization of the RBM in the core region in core−shell architectures. Furthermore, Comsol modeling evidences the impact of the finite rod shape and structure on the vibration modes in the RBM band that significantly differ from pure radial breathing motion. The localization of the acoustic phonons in certain regions of the rod influences their resonant frequency, which together with their spatial overlap with the electron and hole wave functions can be expected to affect coupling to band edge excitons and therefore impact their light emitting properties.

The NCs were synthesized according to published procedures,[18] dispersed in chloroform, and deposited via drop-casting of few microliter solution on 3 × 3 mm large glass substrates. To obtain homogeneous films, the solvent evaporation was carried out in a toluene-saturated atmosphere. ULF Raman measurements[45] were performed under back-scattering configuration at room temperature using a Jobin-Yvon HR800 Raman system, equipped with a liquid-nitrogen-cooled charge-coupled detector (CCD) and a 100× objective lens (numerical aperture ∼0.90). We used a Ti-sapphire laser at 785 nm for excitation, thus with energy below the NC bandgap[18] and under nonresonant conditions. Typical laser power was ∼5 mW. The laser plasma lines were removed using Bragg-volume-grating-based BragGrate bandpass filters from OptiGrate Corp. ULF resolution down to 5 $cm^{-1}$ was achieved by three BragGrate notch filters with optical density of 3 and full width at half-maximum (fwhm) of ∼5−10 $cm^{-1}$. Spectral resolution was ∼0.6 $cm^{-1}$, as estimated from the fwhm of the Rayleigh peak. The accumulation time for each spectrum was ∼300 s. Raman spectra were normalized by the transmittance of the notch filters to improve the peak fitting close to the cutoff frequency. Fitting details are reported in section 1 of the Supporting Information (SI).

Figure 1 shows ULF Raman spectra of CdSe dots and CdS nanorods with 5.7 nm diameter, and CdSe/CdS dot-in-rods with 5.7 nm core- and 5.75 nm rod-diameter. The length of the rods is around 26 nm. The polarization behavior in Figure 1b−d allows to correlate the high frequency band around 13−17 $cm^{-1}$ to symmetric lattice vibrations that appear only in polarized configuration, i.e., excitation polarization parallel to detection polarization, while the low frequency band around 7 $cm^{-1}$ relates to oscillations with substantial asymmetric components that leads to signal also in depolarized measurements, i.e., with excitation polarization perpendicular to detection polarization. The response of the CdSe dots (Figure 1b,e) is well-known and can be understood by fundamental oscillations of an elastic sphere in the frame of Lamb's theory[40,41,46−48] and consists of a RBM in the high frequency band, and ellipsoidal modes in the lower frequency range (see section 2 of the SI for a detailed analysis). For the rods the symmetric mode at high frequency can be associated with a RBM,[43] while the asymmetric low frequency band originates from extensional modes, i.e., oscillations along the long axis of the rod.

Figure 1f shows Lorentz fits to the unpolarized Raman spectrum of CdS rods. The fits reveal peaks at 7.5 and 15.7

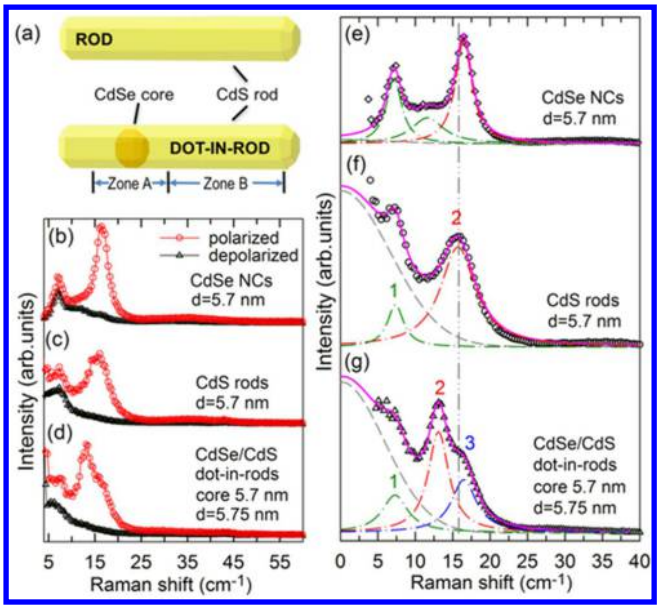


**Figure 1.** Nonresonant Raman spectra of CdS nanorods and CdSe/CdS dot-in-rods with similar diameter and length of 26 nm excited at 785 nm. (a) Illustration of the nanorod and dot-in-rod architectures, where Zone A refers to the region near, and Zone B to the one far away from the core. (b−d) Polarized (red) and depolarized (black) spectra of CdSe cores (b), CdS nanorods (c), and CdSe/CdS dot-in-rods (d) that allow to distinguish between ellipsoidal/extensional (below 12 $cm^{-1}$) and RBM-like vibrations (above 12 $cm^{-1}$). For CdSe nanocrystals (e), the first two peaks result from the ellipsoidal vibrations, while the third peak originates from the RBM (see section 2 of the SI for details). For CdS nanorods (f), two peaks are assigned to the first overtone of the extensional mode and to the RBM. The spectrum of dot-in-rods with 5.7 nm core diameter (g) contains at least three peaks, displaying a dominant redshift of the most prominent Raman peak. The gray dashed line depicts the Raman scattering background near the laser line, and the vertical dashed line indicates the position of the RBM in CdS nanorods. Fitting details are addressed in section 1 of the SI.

$cm^{-1}$ corresponding to the extensional mode and RBM, respectively. The RBM frequency ($\omega_{RBM}$) of a cylinder can be described by[43,49]

$$\omega_{RBM} = \frac{2\tau_n}{D}\sqrt{\frac{E(1-\nu)}{\rho(1+\nu)(1-2\nu)}} \quad (1)$$

with $D$ the diameter of the cylinder, $\nu$ the Poisson ratio, and $\tau_n$ the $n$th root of the equation $\tau J_0(\tau) = \frac{1-2\nu}{1-\nu} J_1(\tau)$. $J_0(\tau)$ and $J_1(\tau)$ are Bessel functions. $\omega_{RBM}$ is dominated by the rod diameter and shows the $1/D$ dependence as in the quantum dot (QD) case. Taking the values of the bulk and shear modulus from ref 50 for CdS as 69 and 14.9 GPa, respectively, we can calculate the Poisson ratio $\nu = 0.4$ and the Young modulus $E = 41.4$ GPa. With these values and the density of CdS as $\rho = 4.82$ g/$cm^3$ we obtain 18 $cm^{-1}$ for $\omega_{RBM}$ in CdS nanorods with 5.7 nm diameter, which is larger than our experimental value (Figure 1c,f). We note that this discrepancy is in line with our data from the CdSe cores (see SI, section 2) that can be accounted for by a reduction of the effective sound velocity $c_l = \sqrt{\frac{E(1-\nu)}{\rho(1+\nu)(1-2\nu)}}$ in NCs by a factor of around 0.8. This reduction could be related to mechanical softening of the nanocrystal surface,[51] which is in line with the reduced Young modulus that we have



DOI: 10.1021/acs.nanolett.6b03706
Nano Lett. 2016, 16, 7664−7670

to use in our finite elements simulations to achieve good agreement for the RBM frequencies of the CdSe cores. Furthermore, the finite length of the nanorods leads to a small redshift of the RBM as we demonstrate in the discussion of the simulations later on. For our nanorods we obtain $c_{l,NR} = 3.57 \times 10^5$ cm/s from $\omega_{RBM}$ in Figure 1f.

The extensional modes are vibrations in direction of the long axis of the rod with frequency

$$\omega_{ext} = \frac{(2n+1)}{L}\pi\sqrt{E_{\parallel}/\rho} \quad (2)$$

where $L$ is the nanorod length. The factor $(2n + 1)$ with $n = 0$, 1, 2, ..., accounts for the number of confined modes.[52] $E_{\parallel}$ is the Young modulus along the long axis of the nanorod. We observe the low energy peak in Figure 1f at 7.5 $cm^{-1}$, which corresponds to the first overtone ($n = 1$) of the extensional mode (7.5 $cm^{-1}$ as ground mode would result in an unrealistically high Young modulus). Taking eq 2 and $n = 1$ we evaluate $E_{\parallel} = 65$ GPa, close to the bulk modulus of CdS (69 GPa). With $E_{\parallel} = 65$ GPa, the extensional ground mode ($n = 0$) is expected at 2.4 $cm^{-1}$, which is not observable because of the cutoff band at ~5 $cm^{-1}$. With $E_{\parallel} = 65$ GPa, we obtain for the sound velocity along the long nanorod axis $c_{l,NR\parallel} = \sqrt{E_{\parallel}/\rho} = 3.67 \times 10^5$ cm/s.

In the spectrum of the CdSe/CdS dot-in-rods in Figure 1g, an additional mode in the RBM band can be identified with respect to CdS nanorods. The most striking feature is the strong peak 2 in Figure 1g that appears at significantly lower frequency (13.1 $cm^{-1}$) than the RBM in bare CdS nanorods (15.7 $cm^{-1}$) and CdSe dots (16.5 $cm^{-1}$). Its polarization behavior (Figure 1d) points to an RBM-like vibration. There is also a high-energy shoulder of peak 2 labeled as peak 3 in Figure 1g at 16.5 $cm^{-1}$, whose polarization behavior allows to assign it to the RBM band.

Figure 2 shows spectra of dot-in-rods with 4.7 nm diameter and different core sizes. For the smallest core (Figure 2a) we observe a single peak in the RBM band at 18.8 $cm^{-1}$ that should be close to the $\omega_{RBM}$ frequency of CdS rods, and indeed using eq 1 with $c_{l,NR} = 3.57 \times 10^5$ cm/s we obtain 18.3 $cm^{-1}$ for $\omega_{RBM}$ of CdS rods with 4.7 nm diameter. For increasing core diameter the dominant peak in the RBM band is red-shifted to 18.1 $cm^{-1}$ (4.0 nm core) and 17.7 $cm^{-1}$ (4.3 nm core), as evidenced in Figure 2b,c. In Figure 2c, a high-energy shoulder of the RBM can be identified by Lorentz fitting, similar as in Figure 1g.

It is well-known that the vibrational modes of QDs shift to higher frequency when embedded in a rigid matrix, such as the CdS nanorod shell, due to rigid boundary conditions.[41] This is opposite to the redshift that we observe for the RBM in dot-in-rods. We therefore have to consider the detailed architecture of the dot-in-rods to analyze the origin of this red shift.

We have performed finite-elements simulations on dots, rods and dot-in-rods to investigate the acoustic vibrations in these architectures (details on the calculations are reported in section 3 of the SI). Such simulations of the vibrations can give insight in the local deformation of the structure and consequently on the symmetry of the vibration modes and the distribution of phonon-induced strain. Figure 3 shows the vibration eigenmodes for the NC shapes discussed in this work. For spherical NCs we obtain the ellipsoidal and RBM mode in very good agreement with Lamb's theory and our experimental results (Figure 3a), if we adjust the Poisson ratio to 0.32 and bulk modulus to 42 GPa, respectively.[53,54] This adjustment of elastic

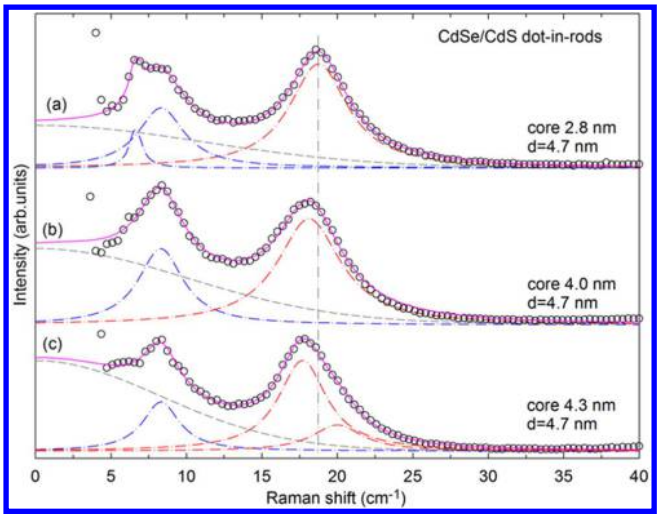


**Figure 2.** (a–c) Unpolarized Raman spectra of dot-in-rods with 4.7 nm diameter and different core sizes. The dominant high-frequency peak exhibits a systematic red shift with increasing core diameter. The vertical dashed line is a guide to the eye marking the center position of the RBM peak in (a), the gray dashed line presents the Raman background. The low-frequency peak at 8.3 $cm^{-1}$ corresponds to the first overtone of the extensional mode. In (a) an additional low-frequency peak was fitted due to the kink close to cutoff. Fitting parameters are reported in the SI in section 1.

parameters of the CdSe dots corresponds to the reduction in sound velocity that is discussed in section 2 of the SI and that was needed for quantitative matching of the observed frequencies in the Lamb's theory analysis. Concerning rods (Figure 3b), taking the bulk values of CdS (Poisson ratio 0.3, and bulk modulus 69 GPa)[50] we find the extensional mode and its higher harmonics in the low frequency region that resemble standing waves along the axis of the cylinder, as expected. Their frequency follows the $1/L$ behavior predicted by eq 2 and as depicted in Figure S7. However, already for the modes in the RBM band we observe strong deviations from just simple radial breathing motion of the rod (in which the rod over its full length would expand and contract): for our rods with finite length the fundamental RBM (F-RBM) at 15.3 $cm^{-1}$ shows a symmetric dilatation/contraction motion located in the central region of the rod. We note that this is still a mainly radially symmetric motion, and therefore, the overall symmetry of this vibration is in agreement with the polarization dependency of the RBM in the Raman experiments (Figure 1c).

The simulation also reveals a second, higher-order RBM (H-RBM) at slightly higher frequency (15.5 $cm^{-1}$) that exhibits a symmetric oscillation off center of the rod. Due to the small splitting in frequency these two modes cannot be discriminated in the experimental spectra, and the vibrational components along the long axis of the rod in the RBMs could explain the weak residual signal in the depolarized Raman spectra of CdS rods. While for rods with infinite length we recover the $1/D$ proportionality of $\omega_{RBM}$ in our simulation, we find that for nanorods with finite length and nanorod diameters from 2 to 6 nm our simulation predicts a small redshift of the F-RBM with respect to eq 1, as demonstrated in Figure S7 in the SI. This effect contributes to the lower F-RBM frequency observed for the nanorods in the Raman experiments in Figure 1f (compared to the prediction of Lamb's theory based on bulk values) and originates from the motion of vibration that is not anymore


DOI: 10.1021/acs.nanolett.6b03706
Nano Lett. 2016, 16, 7664–7670

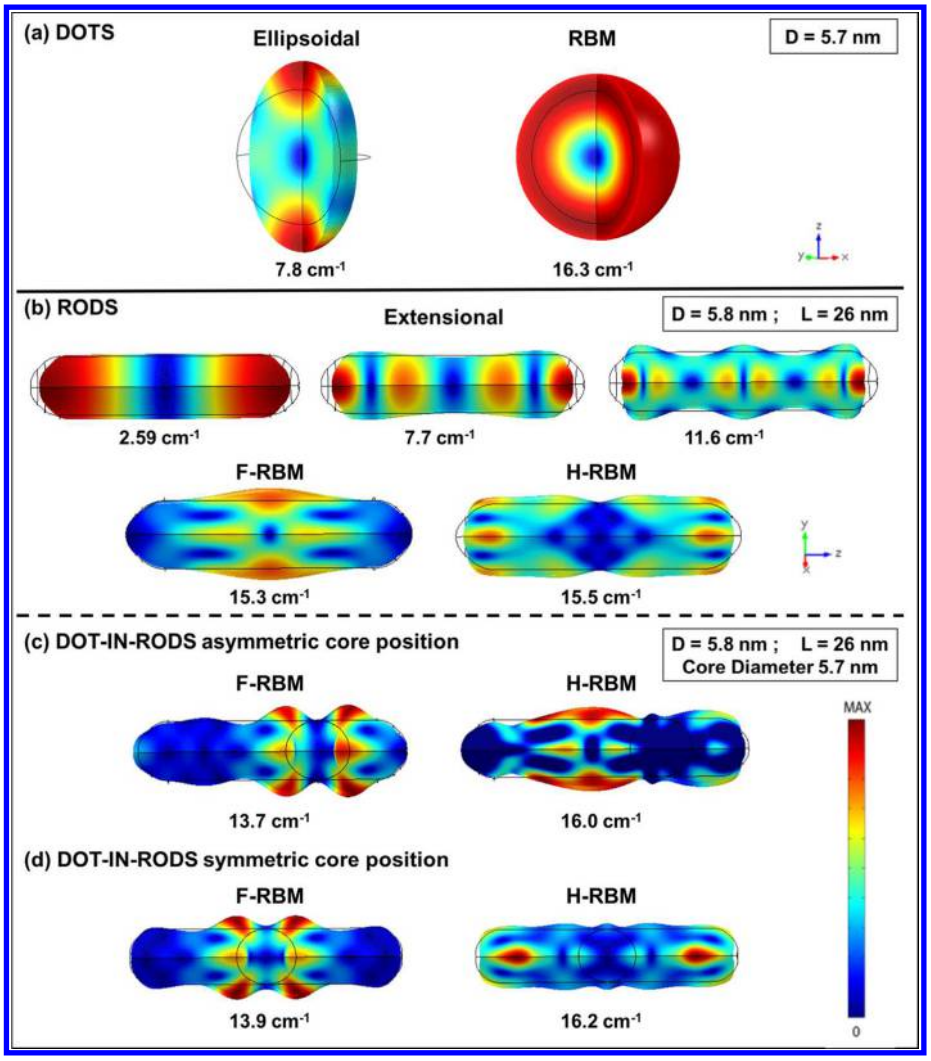


**Figure 3.** Comsol calculations of the deformation of NC spheres (a), rods (b), dot-in-rods with core at 1/3 of their length (c), and symmetric dot-in-rods with the core at their center (d). Deformation magnitude is shown for one maximum of the oscillation and is exaggerated for clarity; blue color corresponds to zero and red to maximum deformation. The thin black lines sketch the outer shape of the NC at rest. The calculated frequency of the modes is stated for each mode. The extensional modes for dot-in-rods are very similar to the ones in rods and are shown in Figure S5 of the SI. A movie showing animated visualizations of the vibrations is provided free of charge.

strictly radial for rods with finite length, which therefore depends also on the elasticity in direction along their *c*-axis.

In comparison to the F-RBM frequency in rods, the simulation shows that the F-RBM frequency in the dot-in-rods is red-shifted because of the presence of the CdSe core, as demonstrated in Figure 3c. This reproduces the redshift of the dominant RBM induced by the core and reveals that the lower-frequency RBM observed at 13.1 $cm^{-1}$ in Figure 1g corresponds to the F-RBM in the dot-in-rods. Interestingly, the symmetry of this vibration mode changes significantly from rods to dot-in-rods. While in rods it is a symmetric expansion/contraction of the central part of the rod, for dot-in-rods the F-RBM is strongly asymmetric, with the maximum deformation concentrated near the core region.

Furthermore, we obtain the H-RBM (Figure 3c) with a significantly increased splitting from the F-RBM in our simulations, which enables its discrimination in the experimental spectra, and thus, we assign the second RBM component observed at 16.5 $cm^{-1}$ in Figure 1g as the H-RBM in the dot-in-rods. The simulated H-RBM in dot-in-rods shows antipodal behavior to the corresponding F-RBM, with the maximum of the oscillation in the CdS section away from the core and minimum deformation in the core region. Both vibration modes consist mainly of oscillation motion in radial direction, which confirms their labeling as RBMs, but have also contributions in axial direction.

The splitting of F-RBM and H-RBM increases with increasing core size, and the small splitting for rods and dot-in-rods with small cores is reflected in the fwhm of the Raman peaks. For example, the fwhm (2.56 $cm^{-1}$) of the RBM peak in rods is much larger than that of the F-RBM in dot-in-rods with large core (1.68 $cm^{-1}$), as depicted in Figures 1f,g. In Figure S6 we report simulation results on dot-in-rods with different core size (that correspond to the structures in Figure 2), which show that the splitting of the two RBM modes increases with increasing core size. This is in good agreement with our experimental results, where the fwhm of the RBM peak increases from 2.8 to 4.0 nm core diameter (see Table S1) and where for the largest cores the splitting of the two modes becomes evident (similar as in Figure 1g).

The core position in dot-in-rods can be exploited to tailor their optical properties, for example, the core could be located



DOI: 10.1021/acs.nanolett.6b03706
*Nano Lett.* 2016, 16, 7664−7670

at the center of the rod.[55] We show the results of such symmetric dot-in-rods in Figure 3d, where the strain for the F-RBM is concentrated again near the core, but now with a symmetric distribution that has a larger number of maxima and minima in deformation as compared to bare rods. Also here the H-RBM has an antipodal strain distribution with respect to the F-RBM.

The extensional oscillations in dot-in-rods are shown in Figure S5 and deviate only slightly from those of monomaterial rods, which is manifested by a very small asymmetry in deformation and a slight reduction in frequency that only becomes evident for the higher order modes. The much smaller impact of the core on the frequency of the extensional modes is related to the nonlocality of this vibration that extends over the full rod volume and therefore is less affected by the local modification of the core.

The finite elements simulations in Figure 3 show that the F-RBM in dot-in-rods (peak 2 in Figure 1g and the corresponding F-RBMs in Figure 2) are localized near the core region. The localization and redshift can also be described in terms of sound velocity in the dot-in-rod heterostructures:

$$c_l = \frac{\omega_{RBM} R}{\tau_l} \tag{3}$$

where $R$ is the radius of the rod. The CdSe core leads to a reduction in sound velocity in the dot-in-rods due to the lower sound velocity in CdSe, and we can write the sound velocity in dot-in-rods (DiR) as $c_{DiR} = c_{CdS} - \Delta c$. Assuming that the reduction is proportional to the volume of the core (with radius $r$) we obtain

$$\begin{aligned} c_{DiR} &= c_{CdS} - \frac{V_{core}}{V_{rod}}(c_{CdS} - c_{CdSe}) \\ &= c_{CdS} - \frac{4/3\pi r^3}{V_{rod}}(c_{CdS} - c_{CdSe}) \end{aligned} \tag{4}$$

Figure 4 shows the experimentally obtained sound velocities (from eq 3) versus $r^3$, and indeed the data is well described by a linear fit. If we consider the full rod volume (with length $L$ = 26 nm) in eq 4 we obtain $c_{CdS} - c_{CdSe} = 3.24 \times 10^5$ cm/s from our data, which is not realistic. Our results in Figure 3c show that the RBM in dot-in-rods is located near the core and that only a certain section of the rod contributes to the vibration. Therefore, we can introduce a parameter $Z$ that describes the effective length within the rod that is affected by the RBM (illustrated by the shaded region in the inset of Figure 4) and use the corresponding volume $V_{Rod,eff} = Z\pi R^2$ in eq 4. With the experimental values for $c_{DiR}$ and by approximating $c_{CdS} - c_{CdSe} \approx 0.8 \times 10^5$ cm/s (which is the difference of the sound velocities in CdS and CdSe) we can obtain an estimate for $Z$, which is around 7 nm. Consequently, also this simplistic modeling based on linear elasticity has to account for the localization of the RBM in the dot-in-rods, and its estimate of localization is in good agreement with the deformation maps obtained by finite elements simulations. Furthermore, the redshift of the F-RBM results from the reduced sound velocity in the core and therefore increases with increasing core diameter. The extensional modes are less affected by this localized reduction of the sound velocity since they are delocalized over the full rod volume.

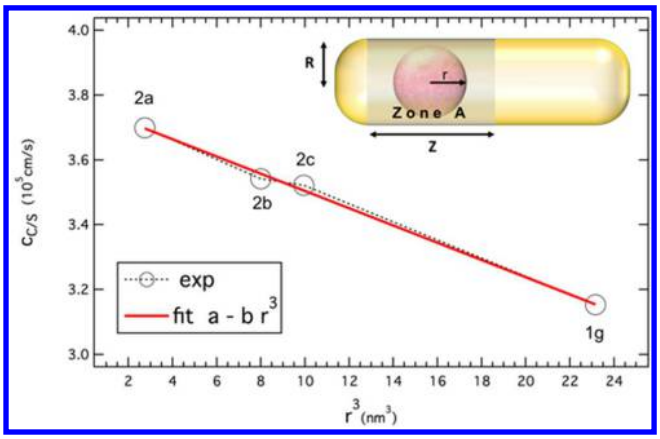


**Figure 4.** Experimental longitudinal sound velocity $c_{c/s}$ in the Zone A of the dot-in-rods versus $r^3$ (open circles). Next to each data point the corresponding spectrum in Figures 1 and 2 is indicated. The red line is a linear fit that yields $a = 3.77 \times 10^5$ cm/s and $b = 0.0266$ cm/(s·nm$^3$). The inset illustrates the geometrical parameters and highlights the Zone A with length $Z$ by gray color.

The above-described localization of phonon-induced strain can be of large interest for the optical properties of nanocrystal heterostructures since acoustic phonons play a crucial role in the transitions between bright and dark exciton states and for the photoluminescence (PL) lifetime.[37] Exciton−phonon coupling should be influenced by spatial overlap, and consequently, we expect faster PL decay for larger cores in dot-in-rods due to the larger region of phonon strain and good overlap with the exciton wave function, which indeed was observed for similar dot-in-rods in refs 23 and 24. We find that the RBM is localized near the core where also the optical band gap transitions occur. Such spatial overlap should enhance exciton−phonon coupling and thereby facilitate transitions to the dark exciton state. Low-energy acoustic excitations in the radiative recombination of dark excitons in dot-in-rods were also observed by Aguila et al.[31] In this letter the authors were puzzled that the acoustic phonon energy could be determined by modeling confined modes in a sphere, while vibrations should be governed by the rod shape. This contradiction can be resolved by our detailed insight into the frequency redshift of the RBM caused by the dot-in-rod architecture that take their structure and finite length into account. We further note that the deformation maps in Figure 3b−d show no coexistence of separate RBM in the core and rod region, as one could naively assume.

In summary, we investigated the acoustic vibrations in nanorods and dot-in-rods by nonresonant Raman spectroscopy and finite elements simulations. Our work goes beyond the standard linear elastic theory approach that considers vibrations in idealized spherical and cylindrical geometries. We reveal that the RBM in dot-in-rods is localized near the core region and that the lower sound velocity in the core region results in a redshift with respect to corresponding bare nanorods. Different core position within the rod leads to different localization of the vibration-induced deformations and affects the magnitude of the red shift. The interplay of strain in NC heterostructures with the vibrational modes[56,57] could be exploited in future to engineer the band structure and exciton−phonon coupling, which opens new opportunities for controlling the light emitting properties.



DOI: 10.1021/acs.nanolett.6b03706
Nano Lett. 2016, 16, 7664−7670

## ■ ASSOCIATED CONTENT

### Supporting Information

The Supporting Information is available free of charge on the ACS Publications website at DOI: 10.1021/acs.nanolett.6b03706.

Details of the fitting to the Raman spectra; confined acoustic phonon modes in CdSe QDs that constitute the cores of the dot-in-rods; finite elements simulations using Comsol software; X-ray diffraction analysis of CdSe/CdS dot-in-rods; transmission electron microscopy images and optical spectra of the nanocrystal samples used in this study (PDF)

Video showing animations of the nanocrystal vibrations (MP4)

## ■ AUTHOR INFORMATION


### Corresponding Authors

*E-mail: phtan@semi.ac.cn.

*E-mail: roman.krahne@iit.it.

### ORCID

Roman Krahne: 0000-0003-0066-7019


### Author Contributions

M.M. and M.L. contributed equally to this work.

### Notes

The authors declare no competing financial interest.

## ■ ACKNOWLEDGMENTS

We thank Dr. Iwan Moreels for fruitful discussions, Francesco De Donato for fabrication of the materials, and Dr. Sergio Marras for X-ray diffraction data. P.H.T. acknowledges support from the National Basic Research Program of China Grant No. 2016YFA0301200, from K. C. Wong Education Foundation, and from the National Natural Science Foundation of China (grants 11225421, 11434010, and 11474277).

## ■ REFERENCES


(1) Bruchez, M.; Moronne, M.; Gin, P.; Weiss, S.; Alivisatos, A. P. *Science* **1998**, *281*, 2013−2016.

(2) Peng, X. G.; Manna, L.; Yang, W. D.; Wickham, J.; Scher, E.; Kadavanich, A.; Alivisatos, A. P. *Nature* **2000**, *404*, 59−61.

(3) Gaponik, N.; Hickey, S. G.; Dorfs, D.; Rogach, A. L.; Eychmüller, A. *Small* **2010**, *6*, 1364−1378.

(4) Kraus, R. M.; Lagoudakis, P. G.; Rogach, A. L.; Talapin, D. V.; Weller, H.; Lupton, J. M.; Feldmann, J. *Phys. Rev. Lett.* **2007**, *98*, 017401.

(5) Gudiksen, M. S.; Maher, K. N.; Ouyang, L.; Park, H. *Nano Lett.* **2005**, *5*, 2257−2261.

(6) Klimov, V. I. *J. Phys. Chem. B* **2000**, *104*, 6112−6123.

(7) Moreels, I.; Raino, G.; Gomes, R.; Hens, Z.; Stöferle, T.; Mahrt, R. F. *Adv. Mater.* **2012**, *24*, OP231−OP235.

(8) Klimov, V. I.; Mikhailovsky, A. A.; Xu, S.; Malko, A.; Hollingsworth, J. A.; Leatherdale, C. A.; Eisler, H. J.; Bawendi, M. G. *Science* **2000**, *290*, 314−317.

(9) Talapin, D. V.; Lee, J. S.; Kovalenko, M. V.; Shevchenko, E. V. *Chem. Rev.* **2010**, *110*, 389−458.

(10) Zavelani-Rossi, M.; Krahne, R.; Della Valle, G.; Longhi, S.; Franchini, I. R.; Girardo, S.; Scotognella, F.; Pisignano, D.; Manna, L.; Lanzani, G.; Tassone, F. *Laser Photon. Rev.* **2012**, *6*, 678−683.

(11) Zavelani-Rossi, M.; Lupo, M. G.; Krahne, R.; Manna, L.; Lanzani, G. *Nanoscale* **2010**, *2*, 931−935.

(12) Grivas, C.; Li, C.; Andreakou, P.; Wang, P.; Ding, M.; Brambilla, G.; Manna, L.; Lagoudakis, P. *Nat. Commun.* **2013**, *4*, 2376.

(13) Guzelturk, B.; Kelestemur, Y.; Olutas, M.; Delikanli, S.; Demir, H. V. *ACS Nano* **2014**, *8*, 6599−6605.

(14) Grim, J. Q.; Christodoulou, S.; Di Stasio, F.; Krahne, R.; Cingolani, R.; Manna, L.; Moreels, I. *Nat. Nanotechnol.* **2014**, *9*, 891−895.

(15) Kim, T.-H.; Cho, K.-S.; Lee, E. K.; Lee, S. J.; Chae, J.; Kim, J. W.; Kim, D. H.; Kwon, J.-Y.; Amaratunga, G.; Lee, S. Y.; Choi, B. L.; Kuk, Y.; Kim, J. M.; Kim, K. *Nat. Photonics* **2011**, *5*, 176−182.

(16) Yang, C.-S.; Kauzlarich, S. M.; Wang, Y. C. *Chem. Mater.* **1999**, *11*, 3666−3670.

(17) Cao; Banin, U. *J. Am. Chem. Soc.* **2000**, *122*, 9692−9702.

(18) Carbone, L.; Nobile, C.; De Giorgi, M.; Sala, F. D.; Morello, G.; Pompa, P.; Hytch, M.; Snoeck, E.; Fiore, A.; Franchini, I. R.; Nadasan, M.; Silvestre, A. F.; Chiodo, L.; Kudera, S.; Cingolani, R.; Krahne, R.; Manna, L. *Nano Lett.* **2007**, *7*, 2942−2950.

(19) Talapin, D. V.; Nelson, J. H.; Shevchenko, E. V.; Aloni, S.; Sadtler, B.; Alivisatos, A. P. *Nano Lett.* **2007**, *7*, 2951−2959.

(20) Sitt, A.; Sala, F. D.; Menagen, G.; Banin, U. *Nano Lett.* **2009**, *9*, 3470−3476.

(21) Krahne, R.; Zavelani-Rossi, M.; Lupo, M. G.; Manna, L.; Lanzani, G. *Appl. Phys. Lett.* **2011**, *98*, 063105.

(22) Sitt, A.; Salant, A.; Menagen, G.; Banin, U. *Nano Lett.* **2011**, *11*, 2054−2060.

(23) Rainò, G.; Stöferle, T.; Moreels, I.; Gomes, R.; Kamal, J. S.; Hens, Z.; Mahrt, R. F. *ACS Nano* **2011**, *5*, 4031−4036.

(24) Rainò, G.; Stöferle, T.; Moreels, I.; Gomes, R.; Hens, Z.; Mahrt, R. F. *ACS Nano* **2012**, *6*, 1979−1987.

(25) Alivisatos, A. P.; Harris, T. D.; Carroll, P. J.; Steigerwald, M. L.; Brus, L. E. *J. Chem. Phys.* **1989**, *90*, 3463−3468.

(26) Cerullo, G.; De Silvestri, S.; Banin, U. *Phys. Rev. B: Condens. Matter Mater. Phys.* **1999**, *60*, 1928−1932.

(27) Son, D. H.; Wittenberg, J. S.; Banin, U.; Alivisatos, A. P. *J. Phys. Chem. B* **2006**, *110*, 19884−19890.

(28) Lange, H.; Artemyev, M.; Woggon, U.; Niermann, T.; Thomsen, C. *Phys. Rev. B: Condens. Matter Mater. Phys.* **2008**, *77*, 193303.

(29) Krauss, T. D.; Wise, F. W. *Phys. Rev. Lett.* **1997**, *79*, 5102−5105.

(30) Yadav, H. K.; Gupta, V.; Sreenivas, K.; Singh, S. P.; Sundarakannan, B.; Katiyar, R. S. *Phys. Rev. Lett.* **2006**, *97*, 085502.

(31) Granados del Águila, A.; Jha, B.; Pietra, F.; Groeneveld, E.; de Mello Donegá, C.; Maan, J. C.; Vanmaekelbergh, D.; Christianen, P. C. M. *ACS Nano* **2014**, *8*, 5921−5931.

(32) Empedocles, S. A.; Norris, D. J.; Bawendi, M. G. *Phys. Rev. Lett.* **1996**, *77*, 3873−3876.

(33) Chilla, G.; Kipp, T.; Menke, T.; Heitmann, D.; Nikolic, M.; Frömsdorf, A.; Kornowski, A.; Föerster, S.; Weller, H. *Phys. Rev. Lett.* **2008**, *100*, 057403.

(34) Fernée, M. J.; Littleton, B. N.; Cooper, S.; Rubinsztein-Dunlop, H.; Gómez, D. E.; Mulvaney, P. *J. Phys. Chem. C* **2008**, *112*, 1878−1884.

(35) Nobile, C.; Fonoberov, V. A.; Kudera, S.; Della Torre, A.; Ruffino, A.; Chilla, G.; Kipp, T.; Heitmann, D.; Manna, L.; Cingolani, R.; Balandin, A. A.; Krahne, R. *Nano Lett.* **2007**, *7*, 476−479.

(36) Lange, H.; Artemyev, M.; Woggon, U.; Thomsen, C. *Nanotechnology* **2009**, *20*, 045705.

(37) Oron, D.; Aharoni, A.; de Mello Donega, C.; van Rijssel, J.; Meijerink, A.; Banin, U. *Phys. Rev. Lett.* **2009**, *102*, 177402.

(38) Rainò, G.; Moreels, I.; Hassinen, A.; Stöferle, T.; Hens, Z.; Mahrt, R. F. *Nano Lett.* **2012**, *12*, 5224−5229.

(39) Lamb, H. *Proc. London Mater. Soc.* **1881**, *s1−13*, 189−212.

(40) Saviot, L.; Champagnon, B.; Duval, E.; Ekimov, A. I. *Phys. Rev. B: Condens. Matter Mater. Phys.* **1998**, *57*, 341−346.

(41) Saviot, L.; Champagnon, B.; Duval, E.; Kudriavtsev, I. A.; Ekimov, A. I. *J. Non-Cryst. Solids* **1996**, *197*, 238−246.

(42) Saviot, L.; Murray, D. B. *Phys. Rev. B: Condens. Matter Mater. Phys.* **2005**, *72*, 205433.

(43) Lange, H.; Mohr, M.; Arternyev, M.; Woggon, U.; Thomsen, C. *Nano Lett.* **2008**, *8*, 4614−4617.

(44) Chen, I.-C.; Weng, C.-L.; Lin, C.-H.; Tsai, Y.-C. *J. Appl. Phys.* **2010**, *108*, 083530.




DOI: 10.1021/acs.nanolett.6b03706
*Nano Lett.* 2016, 16, 7664−7670

(45) Tan, P. H.; Han, W. P.; Zhao, W. J.; Wu, Z. H.; Chang, K.; Wang, H.; Wang, Y. F.; Bonini, N.; Marzari, N.; Pugno, N.; Savini, G.; Lombardo, A.; Ferrari, A. C. *Nat. Mater.* **2012**, *11*, 294−300.
(46) Combe, N.; Huntzinger, J. R.; Mlayah, A. *Phys. Rev. B: Condens. Matter Mater. Phys.* **2007**, *76*, 205425.
(47) Cheng, W.; Ren, S.-F.; Yu, P. Y. *Phys. Rev. B: Condens. Matter Mater. Phys.* **2005**, *71*, 174305.
(48) Tanaka, A.; Onari, S.; Arai, T. *Phys. Rev. B: Condens. Matter Mater. Phys.* **1993**, *47*, 1237−1243.
(49) Hu, M.; Wang, X.; Hartland, G. V.; Mulvaney, P.; Juste, J. P.; Sader, J. E. *J. Am. Chem. Soc.* **2003**, *125*, 14925−14933.
(50) *Landolt-Boernstein Semiconductors*; Springer-Verlag GmbH: Berlin Heidelberg, 1998; Vol. *41b*.
(51) Bozyigit, D.; Yazdani, N.; Yarema, M.; Yarema, O.; Lin, W. M. M.; Volk, S.; Vuttivorakulchai, K.; Luisier, M.; Juranyi, F.; Wood, V. *Nature* **2016**, *531*, 618−622.
(52) Love, A. E. H. *Treatise on the Mathematical Theory of Elasticity*; Dover Publications: New York, 1944.
(53) Zanjani, M. B.; Lukes, J. R. *J. Chem. Phys.* **2013**, *139*, 144702.
(54) Mohr, M.; Caron, A.; Herbeck-Engel, P.; Bennewitz, R.; Gluche, P.; Brühne, K.; Fecht, H.-J. *J. Appl. Phys.* **2014**, *116*, 124308.
(55) Luo, Y.; Wang, L.-W. *ACS Nano* **2010**, *4*, 91−98.
(56) Szilagyi, E.; Wittenberg, J. S.; Miller, T. A.; Lutker, K.; Quirin, F.; Lemke, H.; Zhu, D.; Chollet, M.; Robinson, J.; Wen, H.; Sokolowski-Tinten, K.; Lindenberg, A. M. *Nat. Commun.* **2015**, *6*, 6577.
(57) Christodoulou, S.; Rajadell, F.; Casu, A.; Vaccaro, G.; Grim, J. Q.; Genovese, A.; Manna, L.; Climente, J. I.; Meinardi, F.; Rainò, G.; Stöferle, T.; Mahrt, R. F.; Planelles, J.; Brovelli, S.; Moreels, I. *Nat. Commun.* **2015**, *6*, 7905.



DOI: 10.1021/acs.nanolett.6b03706
*Nano Lett.* 2016, 16, 7664−7670